iScience, Volume *27*

Supplemental information

Superenhancer-driven circRNA Myst4 involves in pulmonary artery smooth muscle cell ferroptosis in pulmonary hypertension

Siyu He, June Bai, Lixin Zhang, Hao Yuan, Cui Ma, Xiaoying Wang, Xiaoyu Guan, Jian Mei, Xiangrui Zhu, Wei Xin, and Daling Zhu

Supplementary Figure legends

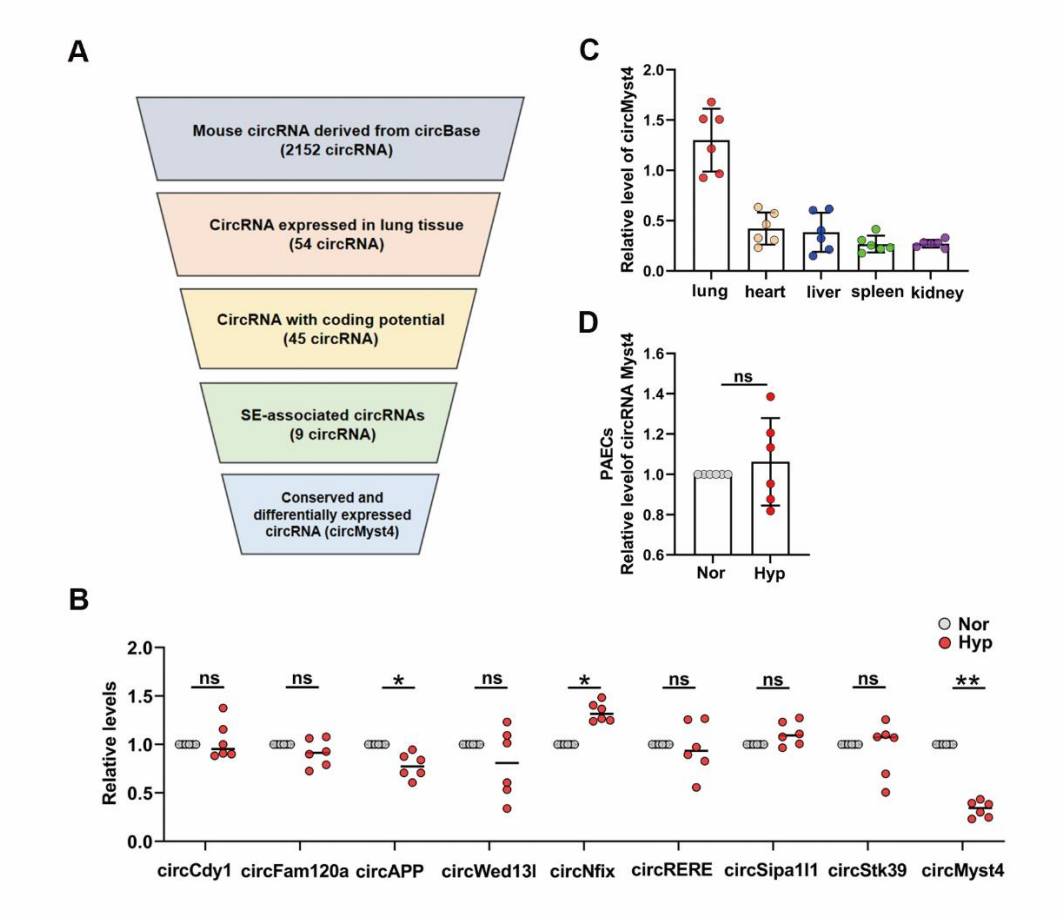

Figure S1. Screening process for circMyst4, related to Figure 1. (A) Flowchart delineating the identification of superenhancer-associated circMyst4 in lung tissue. Firstly, 2152 mouse circRNA derived from circBase database. Then, the intersection of the above circRNAs with the top 100 lung tissue-expressed circRNAs in the CIRCpedia v2 database was performed, and 54 circRNA expressed in lung tissue was screened. After that, 45 circRNAs were screened by predicting the coding potential of the above circRNAs by circBank database. Next, the above circRNAs were analyzed by dbSUPER and SEAv.3.0 database, and 9 superenhancer-associated circRNAs were screened. Finally, by real-time qPCR and conservatism, mmu_circ_0000505 (named as circMyst4) was choose as the target for study. (B) Real-time qPCR analysis of the

expression levels of nine superenhancer-associated circRNAs in hypoxic PASMCs (n=6). (C) Real-time qPCR analysis of the expression levels of circMyst4 in different tissues (n=6 mice/group). (D) Real-time qPCR analysis of the expression levels of circMyst4 in hypoxic pulmonary artery endothelial cells (PAECs) (n=6). Data are shown as means±SD. Statistical analysis was performed with Student's t test. Hyp, hypoxia; Nor, normoxia; ns, not significantly different. $^{*}P<0.05$, $^{**}P<0.01$.

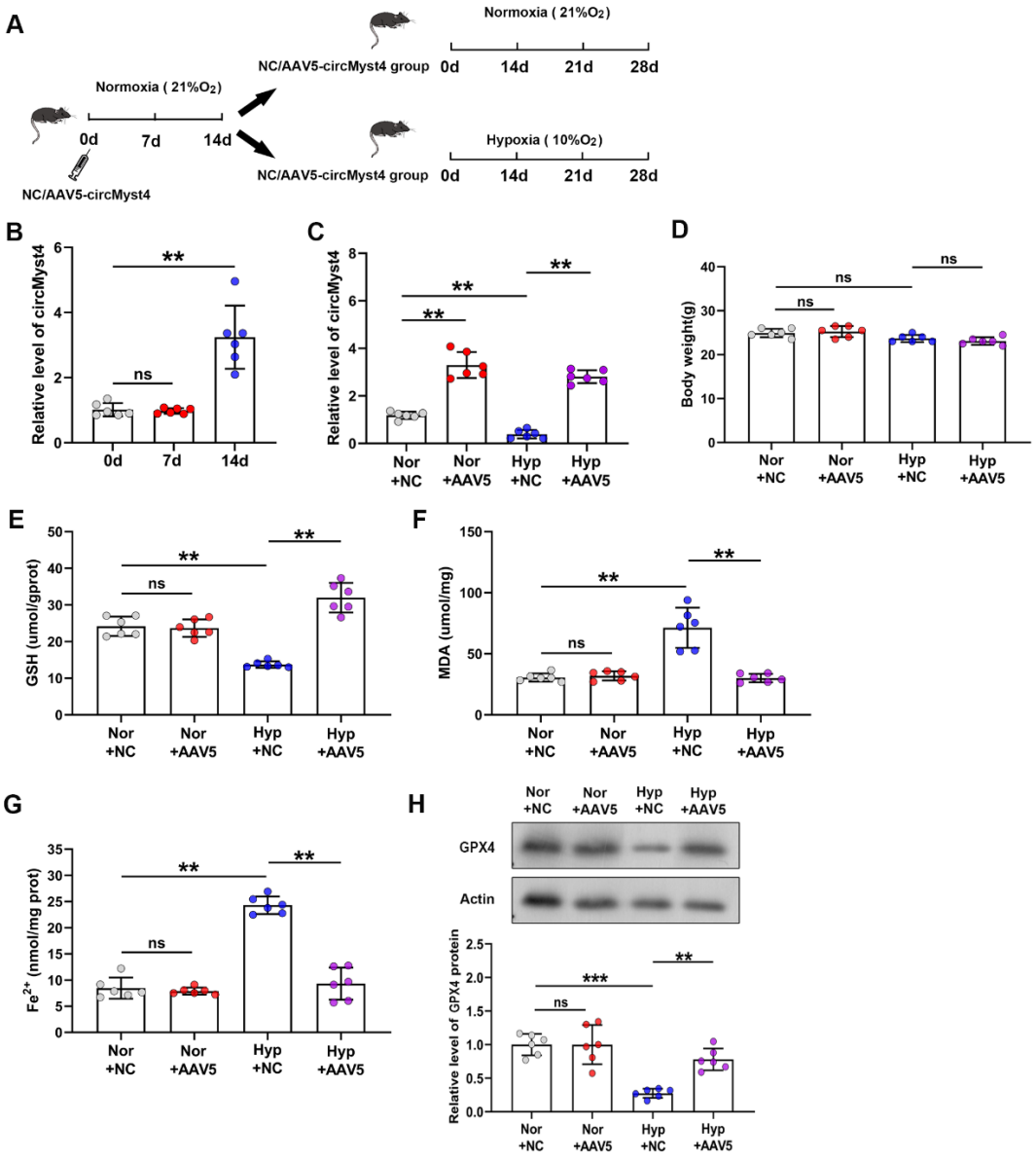

Figure S2. CircMyst4 overexpression significantly inhibits ferroptosis in vivo,

related to Figure 2. (A) The schematic of PH mouse modeling. (B, C) The overexpression efficiency of circMyst4 in vivo (n=6 mice/group). (D) Body weight of mice in different groups (n=6 mice/group). (E-G) Detection of the contents of GSH, MDA and ferrous ion in model mice (n=6 mice/group). (H) Western blotting analysis of GPX4 protein expression (n=6 mice/group). Data are shown as means±SD. Statistical analysis was performed with one-way ANOVA followed by Bonferroni correction. Hyp, hypoxia; Nor, normoxia; NC, negative control; AAV5, serotype 5 adenovirus-associated virus carrying circMyst4; ns, not significantly different; d, day. $^{**}P<0.01$, $^{***}P<0.001$.

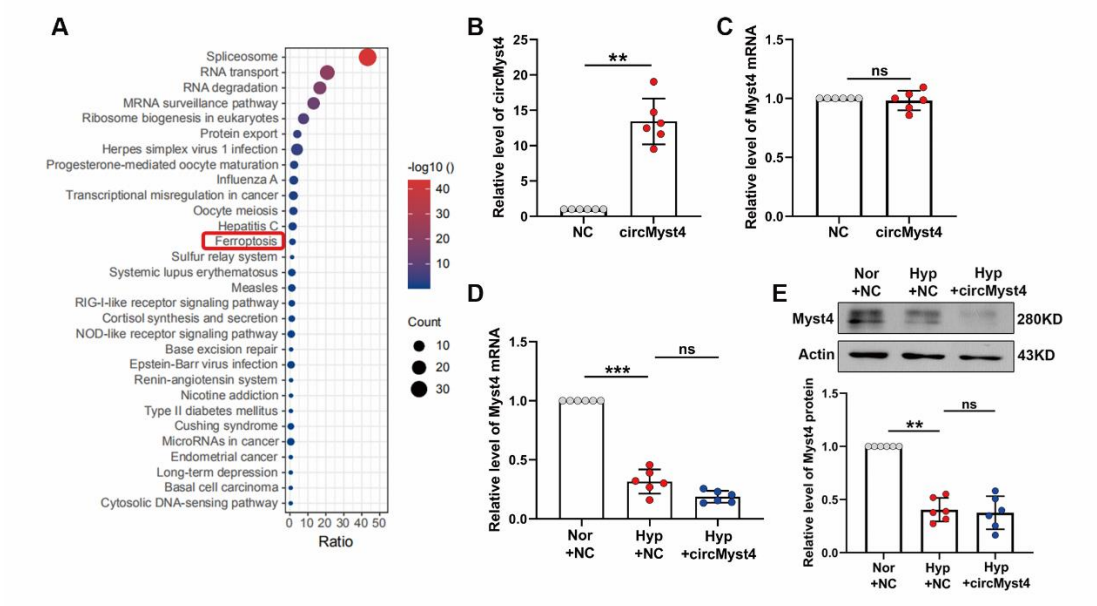

Figure S3. CircMyst4 overexpression has no effect on the mRNA and protein expression of linear Myst4, related to Figure 3. (A) KEGG pathway analysis of genes related to circMyst4. (B) Real-time qPCR analysis of the overexpression efficiency of circMyst4 in PASMCs (n=6). (C-E) After circMyst4 overexpression, real-time qPCR and western blotting analysis of the levels of Myst4 mRNA and protein in PASMCs(n=6). Data are shown as means±SD. Statistical analysis of the graph B and C

was performed with Student's t test. Statistical analysis of the graph D and E was performed with one-way ANOVA followed by Dunn's post-test. Hyp, hypoxia; Nor, normoxia; NC, negative control; ns, not significantly different. $^{**}P<0.01$, $^{***}P<0.001$.

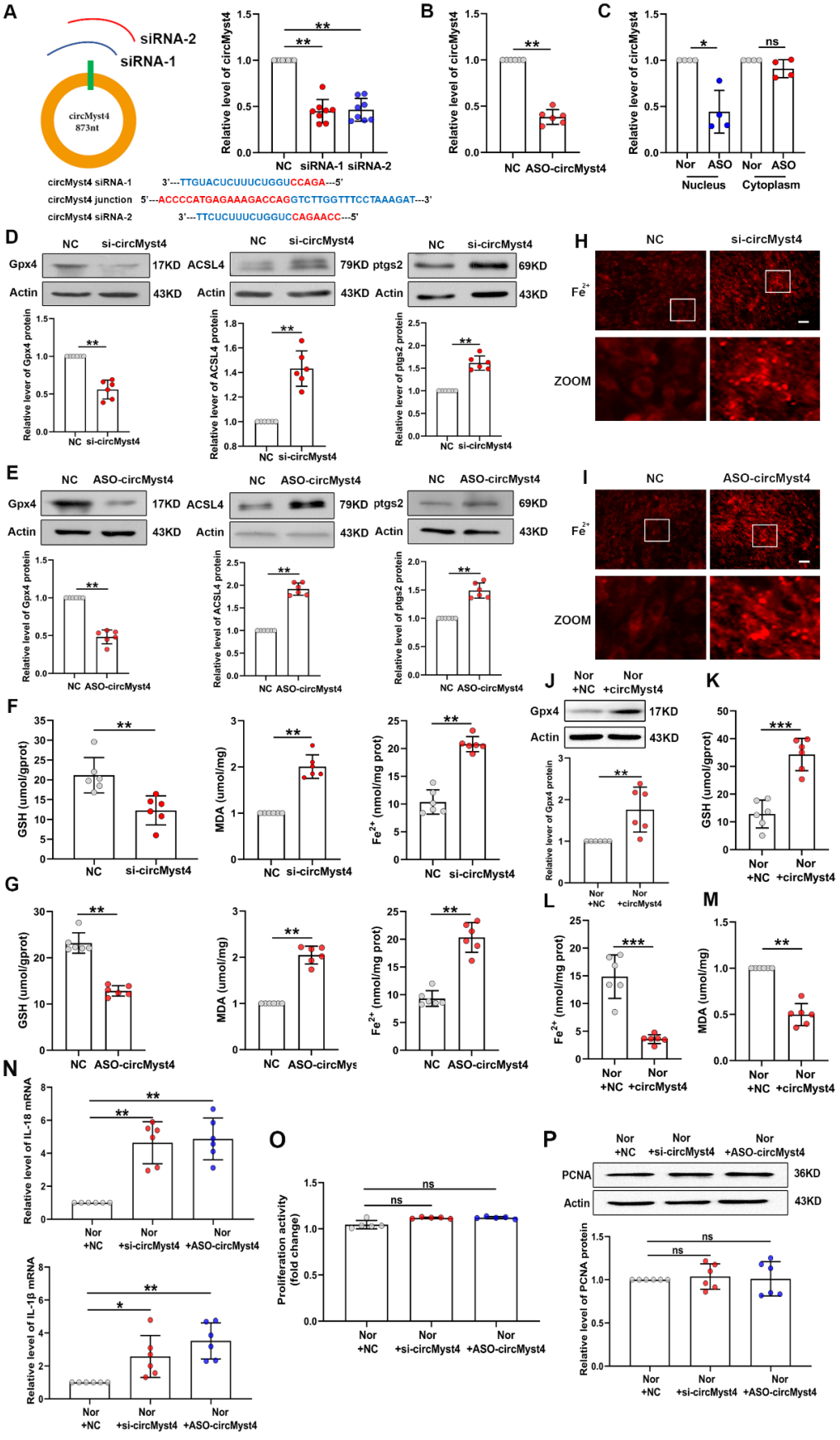

Figure S4. Deficiency of circMyst4 promotes ferroptosis, related to Figure 3. (A-C)

Real-time qPCR analysis of the interference efficiency of circMyst4 (n=4, 6, 8). (D, E) Western blotting analysis of GPX4, ACSL4 and ptgs2 in PASMCs transfected with circMyst4 siRNA or ASO-circMyst4 (n=6). (F, G) After silencing circMyst4, detection of the contents of GSH, MDA and ferrous ion in PASMCs (n=6). (H, I) The percentage of ferrous ion staining-positive cells were detected by a ferrous ion probe (red). Scale bars, 100 μm (n=6). (J) Western blotting analysis of GPX4 in normoxic PASMCs transfected with circMyst4 overexpression plasmid (n=6). (K-M) After overexpressing circMyst4, detection of the contents of GSH, MDA and ferrous ion in normoxic PASMCs (n=6). (N) After knocking down circMyst4, real-time qPCR analysis of the expression of IL-18 and IL-1β (n=6). (O, P) After silencing circMyst4, CCK8 and western blotting analysis of PASMC proliferation (n=5, 6). Data are shown as means±SD. Statistical analysis of the graph A, N, O and P was performed with one-way ANOVA followed by Dunn's post-test. Statistical analysis of the graph C-M was performed with Student's t test. NC, negative control, ASO, antisense oligonucleotide; Nor, normoxia; ns, not significantly different. $^{*}P<0.05$, $^{**}P<0.01$, $^{***}P<0.001$.

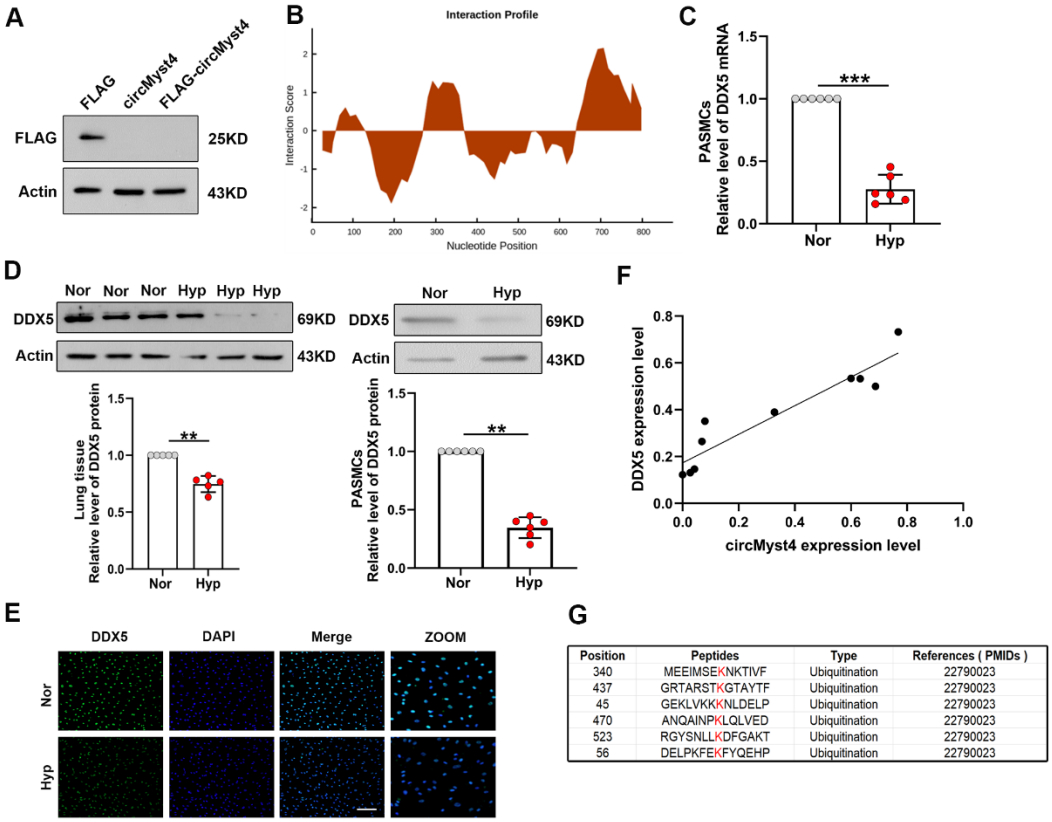

Position	Peptides	Type	References (PMIDs)
340	MEEIMSEKNKTIVF	Ubiquitination	22790023
437	GRTARSTKGTAYTF	Ubiquitination	22790023
45	GEKLVKKKNLDELP	Ubiquitination	22790023
470	ANQAINPKLQLVED	Ubiquitination	22790023
523	RGYSNLLKDFGAKT	Ubiquitination	22790023
56	DELPKFEKFYQEHP	Ubiquitination	22790023

Figure S5. DDX5 is downregulated in hypoxia, related to Figure 4. (A) Western blotting analysis of the expression of FLAG tag protein (n=3). (B) catRAPID database predicted the binding site of circMyst4 to DDX5 (C, D) Real-time qPCR and western blotting analysis of the expression of DDX5 in hypoxic PASMCs (n=5, 6). (E) Immunofluorescence analysis of subcellular localization of DDX5. Scale bars, 100 μm (n=6). Green color denotes DDX5, stained with FITC, and blue color denotes nucleus, stained with DAPI. (F) The correlation analysis of DDX5 with circMyst4 (n=10). (G) Protein Lysine Modifications Database predicted the ubiquitination sites of DDX5. Data are shown as means±SD. Statistical analysis was performed with Student's t test. Hyp, hypoxia; Nor, normoxia; NC, negative control. $^{**}P<0.01$, $^{***}P<0.001$.

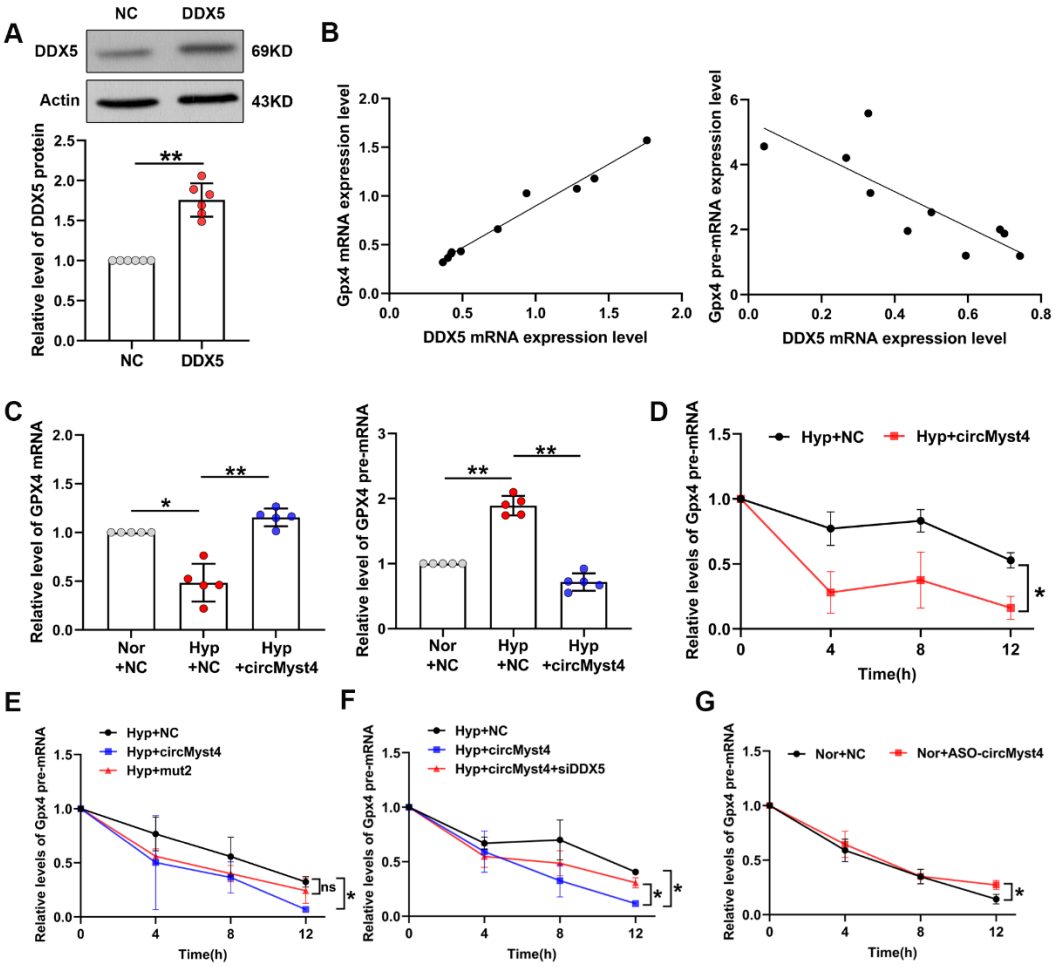

Figure S6. CircMyst4/DDX5 promotes GPX4 mRNA processing, related to Figure 5. (A) Western blotting analysis of the overexpression efficiency of DDX5 in PASMCs (n=6). (B) The correlation analysis of DDX5 with GPX4 and GPX4 pre-mRNA (n=10). (C) After transfection with circMyst4 plasmid, real-time qPCR analysis of the level of GPX4 mRNA and GPX4 pre-mRNA (n=5). (D) After Actinomycin D treatment, real-time qPCR analysis of the impact of circMyst4 overexpression on the stability of GPX4 pre-mRNA (n=3). (E) After Actinomycin D treatment, real-time qPCR analysis of the impact of circMyst4-mut2 overexpression on the stability of GPX4 pre-mRNA (n=3). (F) After Actinomycin D treatment, real-time qPCR analysis of the impact of DDX5 siRNA on the stability of GPX4 pre-mRNA (n=3). (G) After Actinomycin D treatment,

real-time qPCR analysis of the impact of ASO-circMyst4 on the stability of GPX4 pre-mRNA (n=3). Data are shown as means±SD. Statistical analysis of the graph A, D and G was performed with Student's t test. Statistical analysis of the graph C, E and F was performed with one-way ANOVA followed by Dunn's post-test. Hyp, hypoxia; Nor, normoxia; NC, negative control, ns, not significantly different. $^{*}P<0.05$, $^{**}P<0.01$.

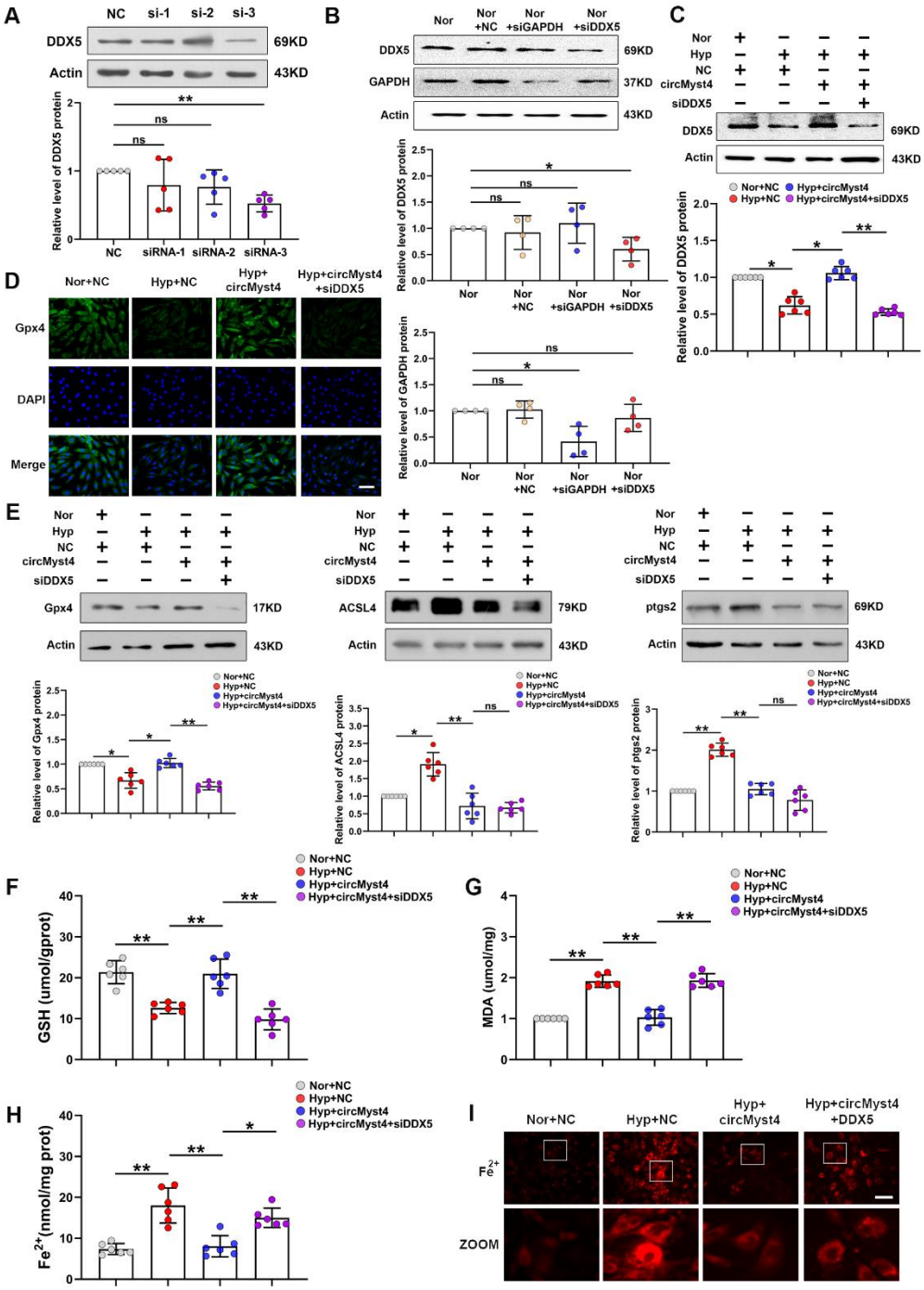

Figure S7. CircMyst4 regulates ferroptosis via the DDX5/GPX4 axis under hypoxic conditions, related to Figure 5. (A, B) Western blotting of the interference efficiency of DDX5 (n=5, 4). (C) Western blotting of the protein levels of DDX5 (n=6). (D) After co-transfection with circMyst4 plasmid and DDX5 siRNA, immunofluorescence analysis of the expression of GPX4. Scale bars, 100 μm (n=6). Green color denotes GPX4, stained with FITC, and blue color denotes nucleus, stained with DAPI. (E) Effects of circMyst4 plasmid and DDX5 siRNA co-transfection on the expression levels of GPX4, ACSL4 and ptgs2 (n=6). (F-H) Effects of circMyst4 plasmid and DDX5 siRNA co-transfection on the content of GSH, MDA and ferrous ion (n=6). (I) After overexpressing circMyst4 and silencing DDX5, detection of the percentage of ferrous ion positive cells. Scale bars, 100 μm. Images of fluorescence staining with a ferrous ion probe (red). Data are shown as means±SD. Statistical analysis of the graph A-E and G was performed with one-way ANOVA followed by Dunn's post-test. Statistical analysis of the graph F and H was performed with one-way ANOVA followed by Bonferroni correction. Hyp, hypoxia; Nor, normoxia; NC, negative control, ns, not significantly different. $^{*}P<0.05$, $^{**}P<0.01$.

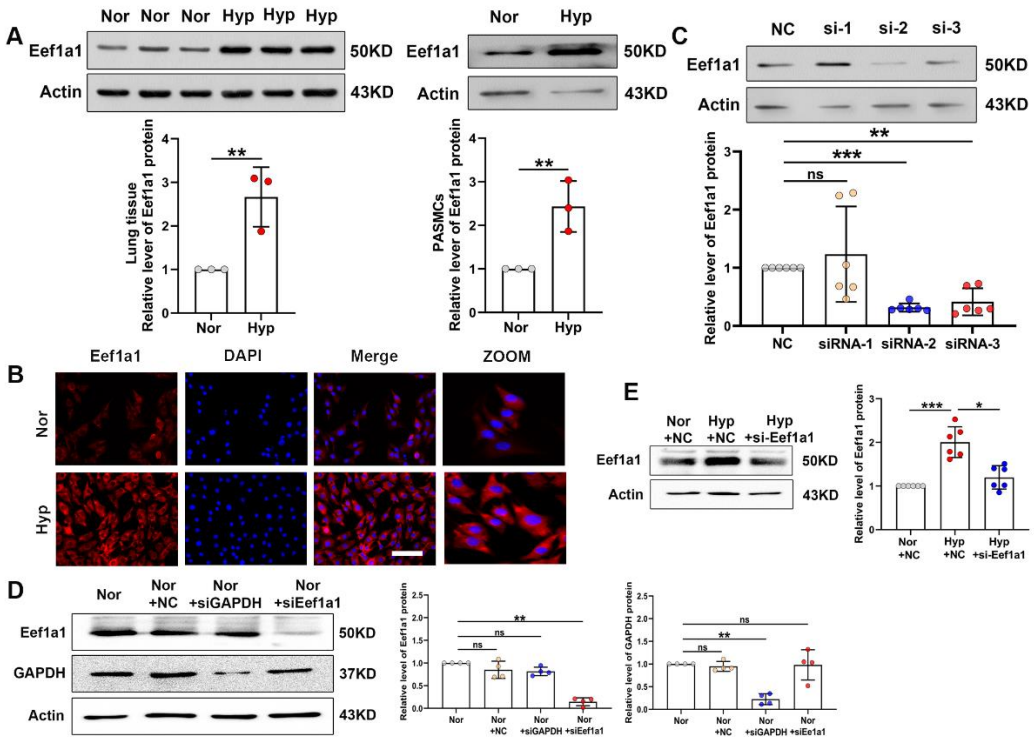

Figure S8. Eef1a1 is upregulated in hypoxia, related to Figure 6. (A) Western blotting of the protein levels of Eef1a1 in hypoxia (n=3). (B) Immunofluorescence analysis of subcellular localization of Eef1a1 in PASMCs. Scale bars, 100 μm (n=6). Red color denotes Eef1a1, stained with Cy3, and blue color denotes nucleus, stained with DAPI. (C, D) Western blotting analysis of the interference efficiency of Eef1a1 (n=6, 4). (E) Western blotting analysis of the protein levels of Eef1a1 (n=6). Data are shown as means±SD. Statistical analysis of the graph A was performed with Student's t test. Statistical analysis of the graph C-E was performed with one-way ANOVA followed by Dunn's post-test. Hyp, hypoxia; Nor, normoxia; NC, negative control; ns, not significantly different. $^{*}P<0.05$, $^{**}P<0.01$, $^{***}P<0.001$.

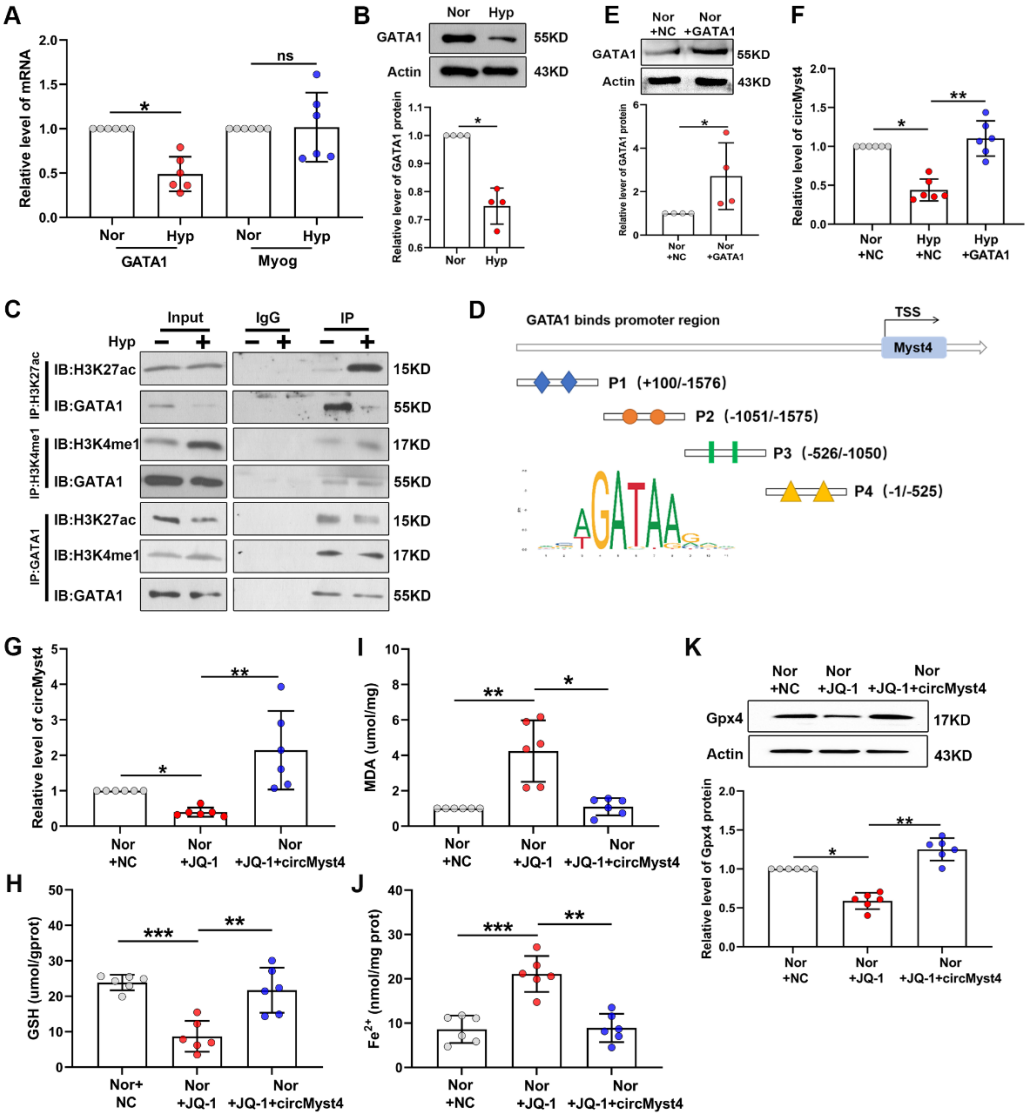

Figure S9. SE is involved in the occurrence of PASMC ferroptosis by regulating circMyst4 expression, related to Figure 7. (A) Real-time qPCR analysis of the expression levels of two candidate transcription factors (n=6). (B) Western blotting analysis of the expression levels of GATA1 (n=4). (C) Co-IP analysis was performed to detect the binding of GATA1 with H3K27ac or H3K4me1. (D) Schematic diagram of GATA1 promoter segmentation. (E) Western blotting analysis of the overexpression efficiency of GATA1 in PASMCs (n=4). (F) After transfection with GATA1 plasmid, real-time qPCR analysis of the level of circMyst4 (n=6). (G) After treatment with JQ-

1 (a superenhancer inhibitor) and circMyst4 plasmid, real-time qPCR analysis of the level of circMyst4 (n=6). (H-J) The GSH, MDA and ferrous ion assays were used to determine the effects of SE and circMyst4 on cell ferroptosis (n=6). (K) Western blotting analysis of effects of SE and circMyst4 on the protein levels of GPX4 in PASMCs (n=6). Data are shown as means±SD. Statistical analysis of the graph A, B and E was performed with Student's t test. Statistical analysis of the graph F, G, I and K was performed with one-way ANOVA followed by Dunn's post-test. Statistical analysis of the graph H and J was performed with one-way ANOVA followed by Bonferroni correction. Hyp, hypoxia; Nor, normoxia; ns, not significantly different. $^{*}P<0.05$, $^{**}P<0.01$, $^{***}P<0.001$.